buildings

MDPI

Article

Study of Mechanical Response of Tunnels Crossing Active Faults in Different Burial Depths

Jiawei Zhang [1,2], Wanhua Zhao [1,*] and Zhen Cui [2]

[1] School of Civil Engineering and Architecture, Wuhan Polytechnic University, Wuhan 430023, China; jiawei991015@gmail.com
[2] State Key Laboratory of Geomechanics and Geotechnical Engineering, Institute of Rock and Soil Mechanics, Chinese Academy of Sciences, Wuhan 430071, China
* Correspondence: zhaowanhuagg@whpu.edu.cn

Abstract: There are numerous tunnels worldwide that cross active fault zones. These tunnels are situated in complex geological environments and are subjected to intense seismic activities. When active fault zones experience displacement, tunnels are susceptible to varying degrees of damage. Over the past few decades, many scholars have researched tunnels crossing active fault zones using numerical simulation methods, including finite element analysis, discrete element analysis, and finite difference methods. However, certain aspects have been overlooked, such as the influence of burial depth on tunnels crossing active fault zones. Most prior studies have primarily omitted consideration of tunnel depth and high-stress effects, resulting in disparities between research findings and practical engineering outcomes. In light of these issues, this paper analyzes the impact of ground stress fields at different burial depths on tunnels crossing active fault zones. It compares the mechanical response characteristics of deep-buried and shallow-buried tunnels after experiencing fault displacement, elucidating variations in displacement patterns, stress, and strain at different burial depths. The results indicate that: (1) Deep-buried and shallow-buried tunnels exhibit an "S"-shaped deformation pattern. (2) Regarding the strain distribution within the tunnel, the affected regions are predominantly concentrated within the fault zone. (3) Regarding the stress distribution within the tunnel, deep-buried tunnels experience a broader range of stress variations distributed across the fault zone. In contrast, shallow-buried tunnels predominantly exhibit stress concentration at the fault slip plane. (4) By analyzing the patterns of tunnel damage at different burial depths, it is observed that burial-depth effects notably influence tunnels with a burial depth less than 200 m. In comparison, tunnels exceeding 300 m gradually reduce the impact of burial depth. These findings can be essential theoretical references for studying tunnels crossing active fault zones in deep-buried environments.

Keywords: fault zone; numerical simulation; tunnel engineering; high stress; mechanical response

check for updates

Citation: Zhang, J.; Zhao, W.; Cui, Z. Study of Mechanical Response of Tunnels Crossing Active Faults in Different Burial Depths. *Buildings* **2023**, *13*, 2723. https://doi.org/10.3390/buildings13112723

Academic Editor: Stefania Sica

Received: 9 October 2023
Revised: 23 October 2023
Accepted: 25 October 2023
Published: 29 October 2023

Copyright: © 2023 by the authors. Licensee MDPI, Basel, Switzerland. This article is an open access article distributed under the terms and conditions of the Creative Commons Attribution (CC BY) license (https://creativecommons.org/licenses/by/4.0/).

1. Introduction

As the global economy develops rapidly, China continues to expand its transport infrastructure, marked by the extensive development of highway and high-speed railway construction throughout the country [1,2]. These massive constructions of highways and railways have also accompanied the emergence of many underground pipeline projects, especially in western China, where the massive construction of highways and railways has generated many highway tunnels, railway tunnels, and water-diversion tunnels. However, China's geology is unique in that active faults are widely distributed, which poses a significant challenge to underground engineering construction. In order to mitigate structural damage caused by active faults to underground pipeline projects, efforts are typically made to avoid crossing active faults wherever possible. Nevertheless, tunnel crossings of active faults may become unavoidable in practical engineering scenarios due to geological and construction constraints, among other factors. Consequently, the investigation of tunnel

failure mechanisms and protective measures across active faults has become imperative to address [3,4].

Fault displacement is a regional geological hazard categorized into two primary forms based on its movement patterns: stick-slip and creep [5–7]. Among these, stick-slip faults accumulate energy from tectonic plate movements and release it suddenly via fault displacement, often resulting in seismic events [8–10].

The 1906 San Francisco earthquake, during which two tunnels traversing the San Andreas fault suffered severe damage [11], exemplifies one instance. Another is the 1999 Chi-Chi earthquake in Taiwan, which substantially harmed numerous nearby tunnels due to dislocations along the Chelongpu fault [12]. The 2008 Wenchuan earthquake also led to extensive tunnel damage along the Duwen expressway near the epicenter [13,14]. Furthermore, the 2016 Kumamoto earthquake in Japan significantly impacted the Toyama tunnel close to the fault [15]. More recently, the 6.9-magnitude earthquake that struck Qinghai, China, in 2022 resulted in substantial damage to the Daliang Tunnel. This tunnel, located near the Cenglong Mountain Fault Zone, experienced fault displacement, with on-site measurements indicating a displacement of up to 2.8 m. As a result, the fault dislocation impact of active faults on tunnels has gained significant attention.

In recent decades, domestic and international scholars have extensively researched the mechanical response characteristics and failure mechanisms of tunnels crossing active faults. In theoretical research, Newmark et al. [16] introduced the theoretical analysis method in 1975 based on the assumption of small displacements for the impact of fault displacement on underground pipelines. Building upon the Newmark–Hall analysis model, Kennedy et al. [17] considered the lateral and longitudinal interactions between soil and pipelines. Yu et al. [18] employed the pseudo-static approach to establish a theoretical analytical model for investigating the influence of surrounding rock stiffness on the seismic response of tunnels. The model was then validated by comparing it with the ABAQUS finite element program results. In numerical simulation, Zucca et al. [19,20] conducted an extensive series of numerical simulations to study the seismic response of a shallow multi-propped underground structure embedded in granular soils. Azizkandi et al. [21] conducted a numerical study to investigate the interaction effects of tunnels on reverse faults and shallow foundations. They analyzed the influence of factors such as ground location, tunnel depth, diameter, and the relative position of the tunnel to the fault zone on the response of shallow foundations to fault rupture under free-field conditions. Using numerical analysis, Banushi et al. [22] examined the influence of different inclinations and internal pressures on the structural response of underground pipelines under strike-slip fault action. Wang et al. [23] used numerical simulations to investigate the internal force response of tunnel lining structures crossing active faults under stick-slip fault action. They proposed an adaptive structural design approach for tunnels crossing active faults. Sabagh et al. [24] studied the failure mechanisms and damage states of tunnels crossing active faults under 60° dip-slip fault action using a 1:60 geometrically similar centrifuge model test in the realm of model experiments. Huang et al. [25] employed non-contact digital image correlation (DIC) technology in a physical model test (3 m × 2.4 m × 0.4 m) to research the failure mechanisms of tunnels near fault zones. Wang [26] conducted model experiments to explore the deformation and damage of overlying soil and its impact on tunnels under standard fault displacement. Zhang et al. [27] conducted a comparative analysis to examine the mechanical performance differences between traditional tunnel structures and flexible-joint tunnel structures. They identified the tunnel lining structure's cracking range, damage characteristics, and failure modes. Zhou [28] investigated the deformation and failure mechanisms of flexible-joint underwater tunnels under strike-slip fault offset using model experiments.

Based on the research mentioned above, it is evident that these studies have yet to consider tunnel depth and have overlooked the influence of in situ stress. However, in practical engineering, the impact of in situ stress conditions on rock displacement is a significant factor, especially in areas with more complex geological conditions at greater

depths. Therefore, researching deep-buried tunnels crossing active fault zones has become a crucial scientific issue that must be addressed in underground engineering construction.

This paper utilizes Abaqus CAE/2022 finite element analysis software to establish a three-dimensional nonlinear model to address the current research gap in studying deep-buried tunnels crossing active fault zones. It compares the distinctions in the failure mechanisms between deep-buried and shallow-buried tunnels when subjected to fault displacement. Additionally, it analyzes the variations in displacement patterns, stress, and strain resulting from fault displacement under different burial conditions. Finally, the paper recommends fault mitigation measures for deep-buried and shallow-buried tunnels.

2. Engineering Background and Finite Element Model

2.1. Project Overview

The Xianglushan Tunnel is located in Yunnan Province, China, and is a crucial structure in the first section of the Dianzhong Water Diversion Project, traversing the Ma'er Mountains. As shown in Figure 1, the Xianglushan Tunnel crosses multiple Holocene active fault zones and encounters a complex geological environment, which results in a higher risk profile. This study focuses on the Xianglushan Tunnel within the context of the Dianzhong Water Diversion Project. The tunnel crosses the Longpan-Qiaohou (F10-1) fault zone prototype, which has experienced cumulative horizontal displacement of up to 0.4 m over the past century. The tunnel features a circular cross-section with a radius of 5.65 m, and its initial lining is constructed using C25 concrete, while the secondary lining is made of C30 concrete.

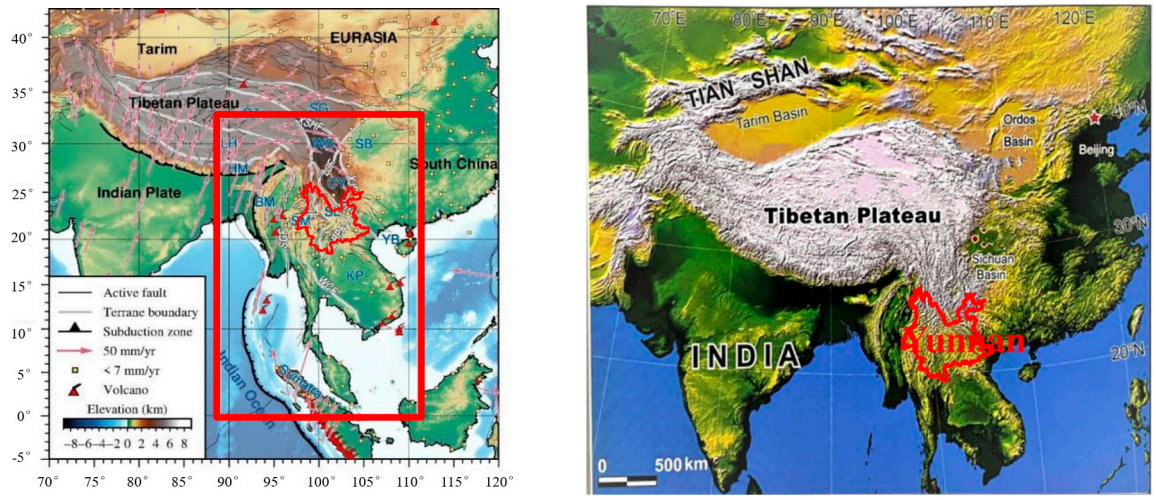

(**a**)

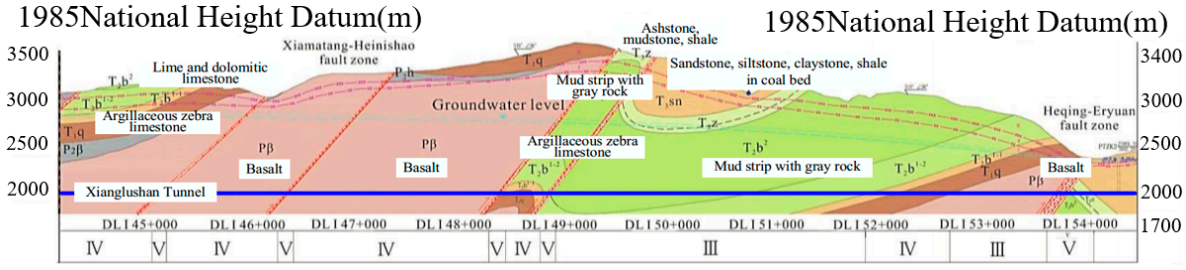

(**b**)

Figure 1. Overview of Xianglushan Tunnel. (**a**) Geographic location of Yunnan Province. (**b**) Stratigraphic profile of Xianglushan Tunnel.

2.2. Finite Element Model Analysis

A three-dimensional numerical model was established using Abaqus software, and numerical simulations were conducted. As shown in Figure 2, after a comprehensive analysis of various structural factors related to real-world engineering faults, the parameters for this calculation were determined as follows: fault dip angle of 90°, fault width of 200 m, tunnel depth of 100 to 1200 m, and the dimensions of the three-dimensional numerical model were set at 200 × 200 × 600 m. As shown in Figure 3, the tunnel lining has a circular cross-section consisting of an initial support with a thickness of 25 cm and a secondary lining with a thickness of 80 cm. In the numerical simulation, the Geological Structure Method is employed, and special attention is paid to the response characteristics of the tunnel lining when analyzing the interaction between the faults and the tunnel. At the same time, to ensure the accuracy and efficiency of the calculations, a finer mesh has been employed for the rock mass within the fault zone and in the vicinity of the tunnel. The remaining rock mass employs a relatively coarse grid. The tunnel lining employs a refined grid in the sections where the tunnel intersects fault zones and their perimeters.

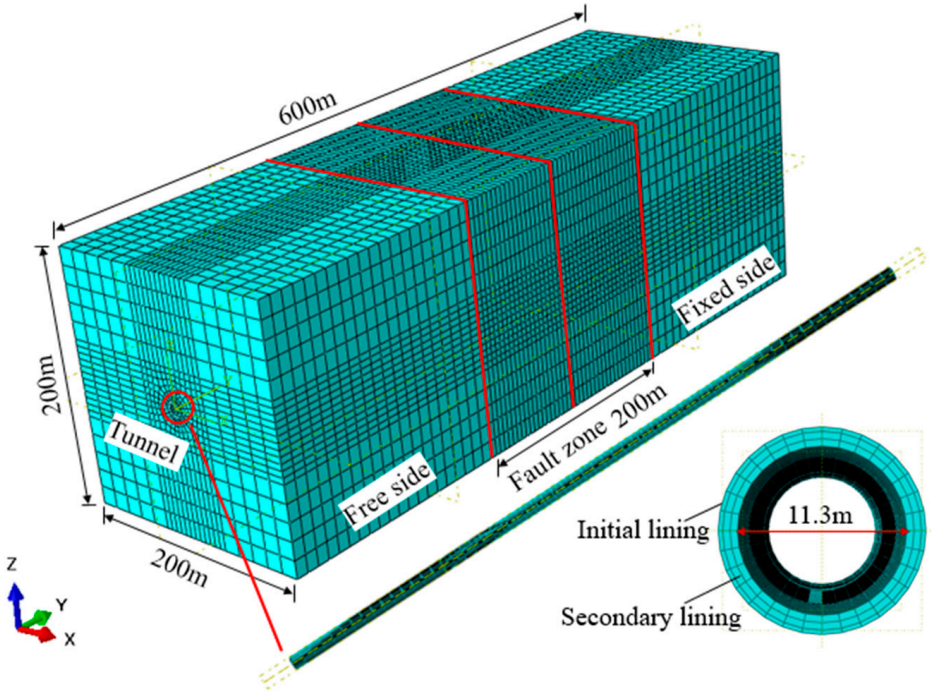

Figure 2. Three-dimensional numerical model.

The numerical model represented the rock mass and the lining using C3D8R hexahedral elements. The rock mass was assumed to exhibit elastoplastic behavior, and the elastoplastic constitutive model for the rock mass followed the Mohr–Coulomb yield criterion. Considering the potential separation between the surrounding rock and the lining due to fault movement, a separable approach was employed in the average direction. It means that when the contact pressure becomes zero or negative, the two contact surfaces separate, removing the contact constraint between them. In the tangential direction, the shear behavior of the interface can be modeled by the Coulomb friction law, which can be expressed as:

$$\tau_{crit} = \mu p \quad (1)$$

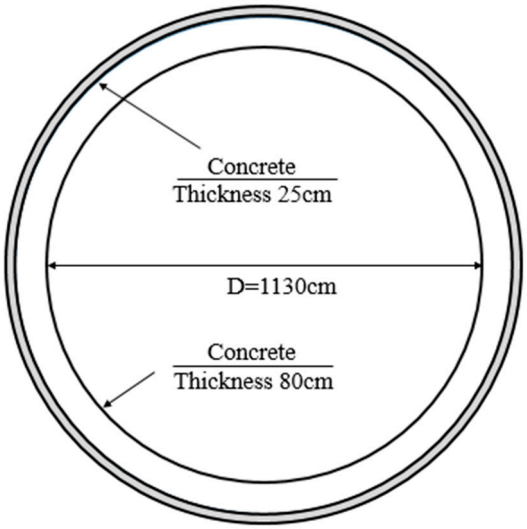

Figure 3. Tunnel cross-section structural diagram.

In this study, it is assumed that the friction coefficient μ between the surrounding rock and the lining is 0.6 [29]. Where τ_{crit} is the critical value of the contact shear stress, μ is the friction coefficient, and p is the contact compressive stress. The slip in the tangential direction remains zero until the contact shear stress reaches the critical value τ_{crit}.

Because the permanent deformation of the surrounding rock induced by fault displacement is the primary cause of tunnel lining damage, a pseudo-static method was employed to apply fault displacement in the X-direction when calculating the response of the tunnel lining under the influence of active fault displacement. Tunnel excavation and support are taken into account during the construction process. In the analysis, the top boundary was defined as a stress boundary to simulate the gravitational effects of the overlying rock strata, while the remaining boundaries were considered displacement boundaries. Stress magnitudes were determined based on the overlying deep-seated rock and soil self-weight. The fault-tunnel 3D numerical model analysis involves three main steps: (1) Initial Ground Stress Equilibrium: The initial step establishes the equilibrium of ground stresses in the model. (2) Tunnel Excavation: This step simulates the tunnel excavation and is often simplified as instantaneous excavation from one side to the other. (3) Application of Fault Displacement: In this step, fault displacement is applied to the model to simulate the fault's movement (movement process).

In the numerical model, the rock body is assumed to be elastic-plastic material, and the lining is assumed to be elastic material; the mechanical parameters in this numerical model refer to the values of the parameters in the actual engineering report, and the specific physical and mechanical parameters are shown in Table 1.

Table 1. Mechanical parameters in the numerical model.

	Density/(kN·m^{-3})	Elastic Modulus/GPa	Poisson's Ratio	Cohesion/MPa	Internal Friction Angle/(°)
Intact rock mass	25.50	7.50	0.28	0.55	33.2
Fault fracture zone	17.00	0.90	-	0.15	25.00
Initial lining	25.00	28.00	0.2	-	-
Secondary lining	25.00	30.00	0.20	-	-

2.3. Computational Approach

Referring to the simulation environment established by Zhou et al. [30], horizontal tectonic stress was applied at the model's level, while vertical stress represented the overlying rock layers' gravitational force. The ratio of simulated horizontal stress to vertical

stress was set at 0.8. In motion and time, a constant velocity displacement was imparted to the active fault to simulate creep-style fault movement. The calculated period covered a 100-year engineering service life. Eight distinct simulation scenarios were designed to investigate the impact of fault rupture on tunnels crossing at various burial depths, as outlined in Table 2. Figure 4 illustrates a schematic representation of the deformation of the surrounding rock and lining for tunnel displacement in response to these different burial depths.

Table 2. Simulation scenarios.

Simulation Conditions	Displacement/m	Fault Zone Width/m	Tunnel Depth/m
1	0.1/0.2/0.3/0.4	200	100
2	0.4	200	200
3	0.4	200	300
4	0.4	200	400
5	0.4	200	600
6	0.4	200	800
7	0.4	200	1000
8	0.1/0.2/0.3/0.4	200	1200

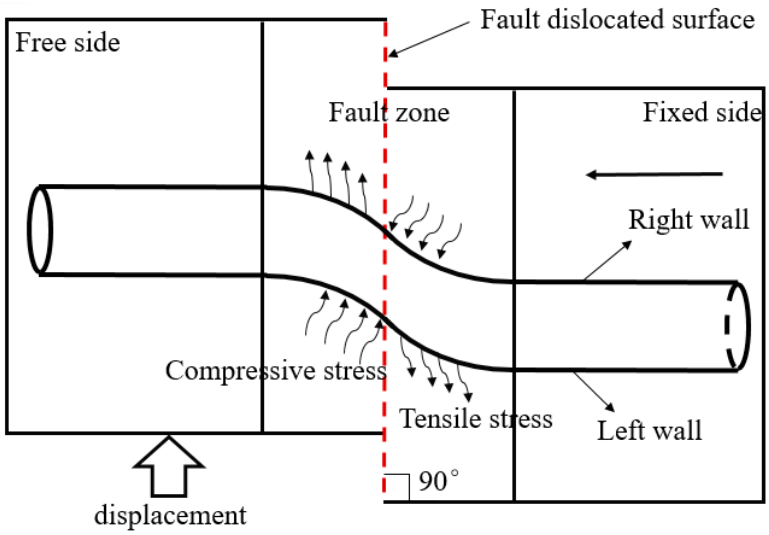

Figure 4. Illustration of surrounding rock-lining deformation.

3. Analysis of the Effects of Fault Displacement on Deep-Buried and Shallow-Buried Tunnels

In order to comprehensively investigate the differences in the mechanical responses of deep-buried and shallow-buried tunnels subjected to strike-slip fault displacement, an analysis was conducted on the displacements, stresses, and strains of the tunnel secondary lining under different fault displacements for Cases 1 and 8.

3.1. The Influence of Different Displacement Amounts on Tunnel Deformation

Figure 5 illustrates the deformation curves for shallow-buried and deep-buried tunnels under different fault displacement levels for Cases 1 and 8. From the deformation patterns, it can be observed that the secondary lining on the fixed side experiences minimal influence from fault displacement, and no displacement deformation is evident. The inner tunnel exhibits a curved deformation pattern within the fault zone interval, with relatively minor variations near the fixed side and more significant variations near the free side. Moreover, the leftmost section of the fault zone closely approaches the applied fault displacement value. Additionally, on the free side, the secondary lining displacements under different

fault displacement conditions show consistency with the fault displacement values, with minimal variation along the longitudinal direction of the lining.

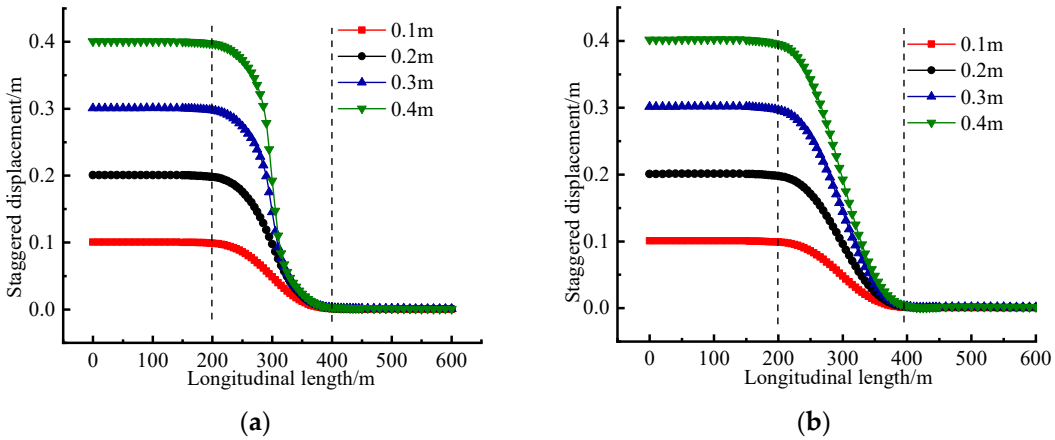

Figure 5. Displacement characteristics of deep-buried and shallow-buried tunnels. (**a**) Tunnel depth of 100 m. (**b**) Tunnel depth of 1200 m.

Figure 6 displays displacement contour plots for deep-buried and shallow-buried tunnels. A comparative analysis reveals that both types exhibit an "S"-shaped deformation pattern, with localized bending occurring at the deformation zone. Notably, shallow-buried tunnels exhibit significantly larger bending angles than their deep-buried counterparts. Regarding deformation trends, it becomes apparent that shallow-buried tunnels experience more pronounced deformation, albeit to a smaller extent. In contrast, deep-buried tunnels display a broader range of deformation distribution, resulting in a more considerable overall extent of damage.

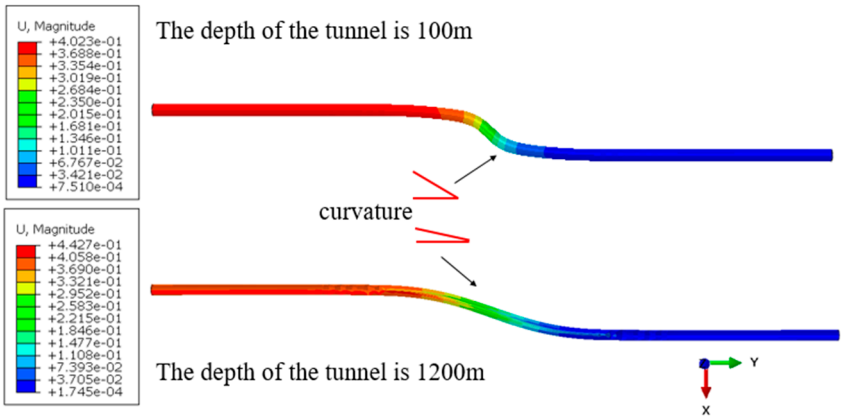

Figure 6. Displacement contour maps for deep-buried and shallow-buried tunnels.

3.2. Strain Distribution in Tunnels under Varying Displacement Levels

Figure 7 illustrates the variations in strain along the left and right walls of shallow-buried and deep-buried tunnels at different fault displacement levels. Positive values represent tensile strains, while negative values indicate compressive strains. As the fault displacement increases, the strain on the left and right tunnel walls continues to rise, with the most significantly affected areas primarily concentrated in the middle of the fault zone. When the tunnel is affected by strike-slip dislocation, the left wall of the lining on the free side is dominated by compressive strain, the right wall is dominated by tensile strain, the left wall of the lining on the fixed side is dominated by tensile strain, and the right wall is dominated by compressive strain.

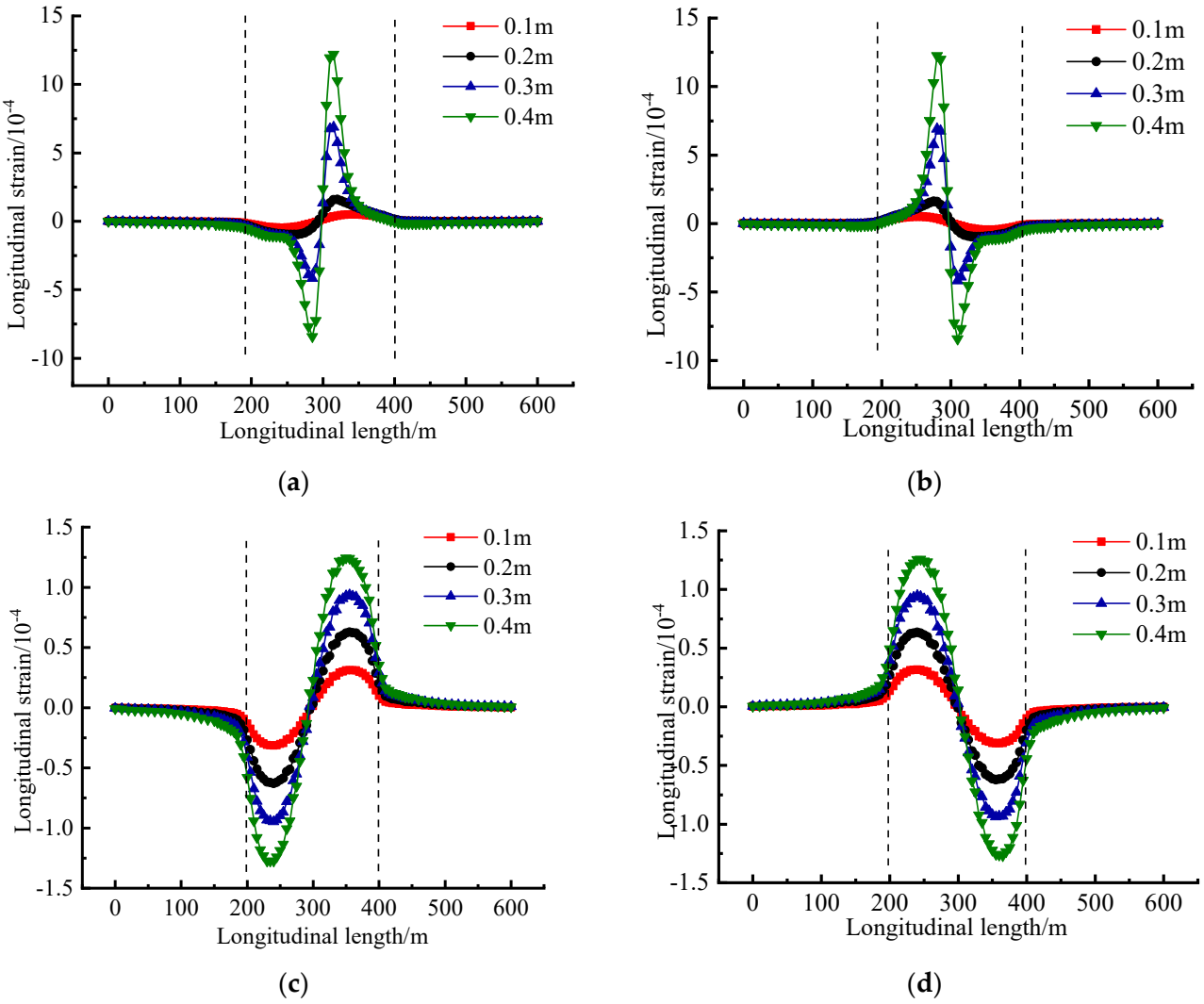

Figure 7. Strain characteristics of deep-buried and shallow-buried tunnels. (**a**) Left tunnel wall at a burial depth of 100 m, (**b**) right tunnel wall at a burial depth of 100 m, (**c**) left tunnel wall at a burial depth of 1200 m, (**d**) right tunnel wall at a burial depth of 1200 m.

Although the strain law of shallow-buried tunnels is the same as that of deep-buried tunnels, the strain distribution range of both is different. The strain distribution of shallow-buried tunnels is more concentrated, while that of deep-buried tunnels is more dispersed.

In order to further analyze the strain distribution patterns during the fault displacement process, Figure 8 compares strain patterns in the tunnel lining at the fault zone after a 0.4 m displacement. It highlights differences in the damaged areas of the lining influenced by different in situ stress conditions for tunnels at varying burial depths. In shallow-buried tunnels, strain primarily concentrates around the fault dislocation surface, whereas in deep-buried tunnels, strain distribution is more extensive, with fewer occurrences near the fault dislocation surface. Consequently, deep-buried tunnels experience less influence from fault displacement. As the burial depth increases, the in situ stress within the surrounding rock mass also rises. Higher in situ stress results in more significant constraints on tunnel lining deformation, making it less prone to deformation.

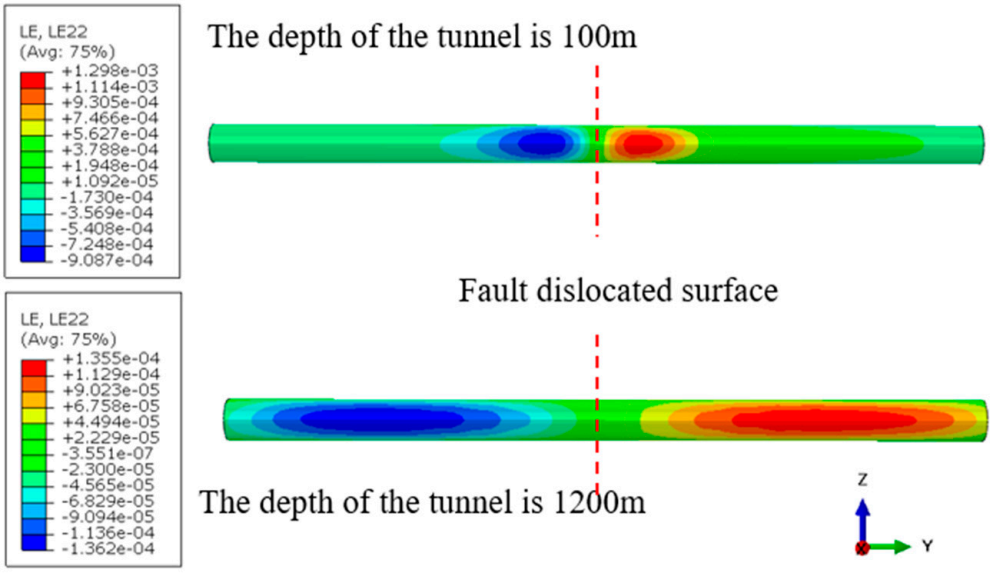

Figure 8. Strain characteristics of deep-buried and shallow-buried tunnels.

By considering the displacement patterns of tunnels, we can deduce that tunnel damage tends to be more severe in shallow-buried environments, primarily concentrated near the fault-dislocated surface. In contrast, the damage extends over a wider area for deep-buried tunnels. Based on these distinct damage patterns, it becomes evident that, in practical engineering, it is necessary to establish longer fault-resistant zones for deep-buried tunnels.

3.3. The Impact of Varying Fault Displacement on Tunnel Stress

Figures 9 and 10 illustrate the longitudinal distribution curves of the principal stresses on the left and right tunnel walls under deep-buried and shallow-buried conditions, with tensile stress considered positive and compressive stress as unfavorable. Due to the weaker rock properties near the fault zone, most of the stress variations occur within the fault zone. When the tunnel is buried at a depth of 100 m, the minimum and maximum principal stresses are 27.6 MPa and 37.1 MPa, respectively. However, at a tunnel depth of 1200 m, the minimum and maximum principal stresses are 4.17 Mpa and 4.23 MPa, respectively. When the maximum principal stress in the tunnel exceeds the ultimate tensile strength of C30 concrete, and the minimum principal stress surpasses the ultimate compressive-tensile strength of C30 concrete, the tunnel lining undergoes damage. According to the Chinese Code for Design of concrete structures (GB 50010-2010) [31], C30 concrete has an ultimate tensile strength of 2.01 MPa and an ultimate compressive strength of 20.1 MPa. By monitoring the stress variations within the tunnel, it is evident that both shallow-buried and deep-buried tunnels experience lining damage when the fault slip reaches 0.2 m, at which point the tunnel lining has reached the ultimate tensile strength of C30 concrete, indicating structural failure.

Via the above numerical simulation, the damaged form of the tunnel lining can be identified as shear tensile damage. The tunnel lining resisted the movement of the movable disc during the slip movement, and the lining of the left and right walls in the axial direction produced significant tensile and compressive stresses. When the tensile and compressive stresses exceed the lining strength, the lining produces shear tensile damage. This type of damage is lining damage, the more common form of damage in the early deformation stage, and the faults are minor. In the early deformation stage, the amount of fault misalignment and the tunnel force are small. This stage is mainly the position of the misalignment surface lining damage, with the increase in the amount of misalignment of shear tensile damage gradually expanding.

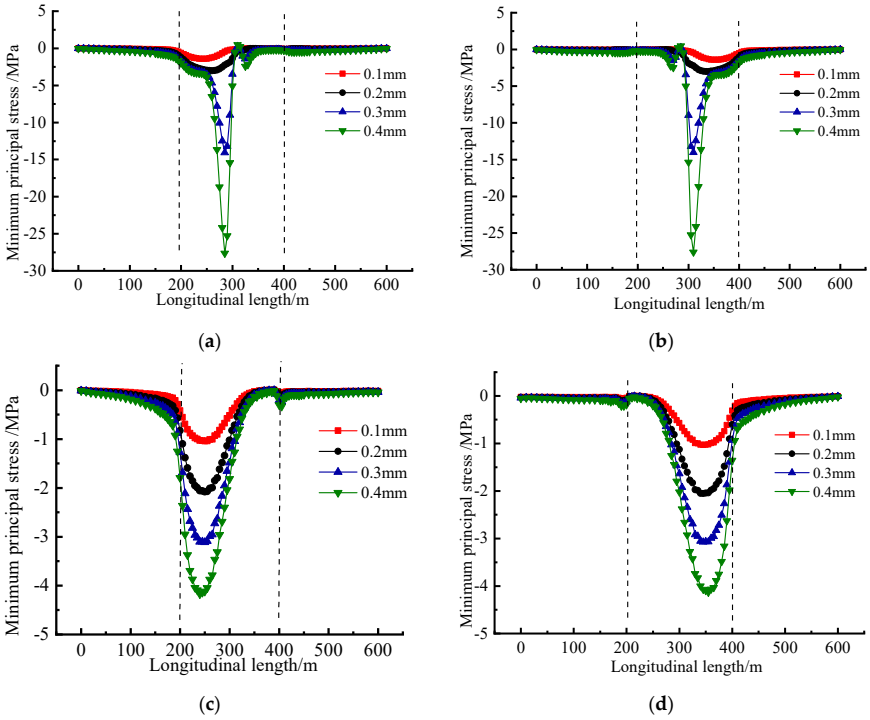

Figure 9. Variations in the minimum principal stress. (**a**) Minimum principal stress on the left wall of the 100 m deep tunnel, (**b**) minimum principal stress on the right wall of the 100 m deep tunnel, (**c**) minimum principal stress on the left wall of the 1200 m deep tunnel, (**d**) minimum principal stress on the right wall of the 1200 m deep tunnel.

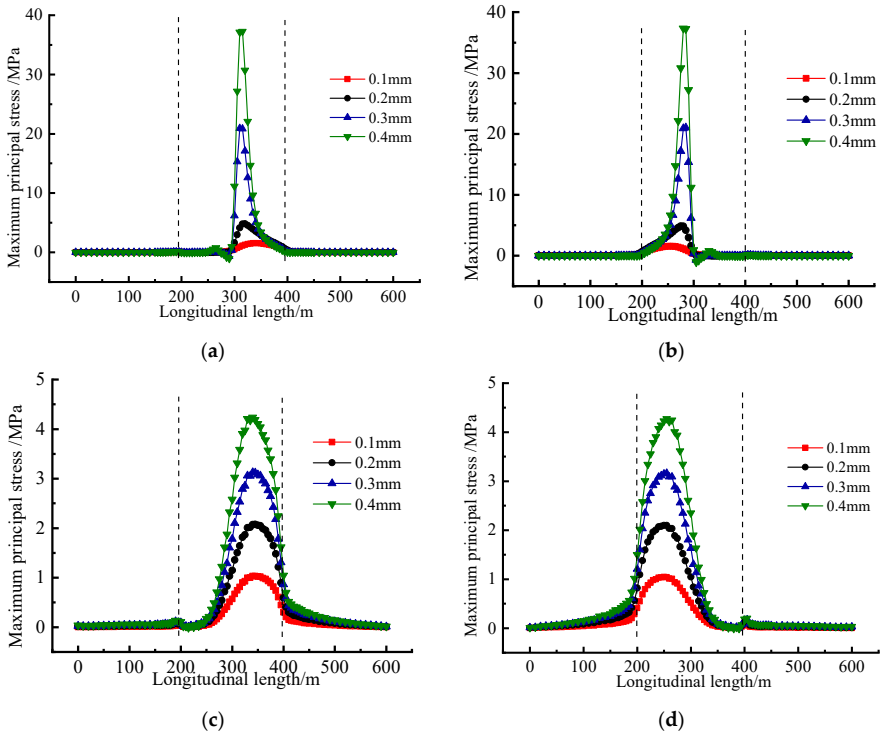

Figure 10. Variation in maximum principal stress characteristics. (**a**) Maximum principal stress on the left wall of the tunnel at a depth of 100 m, (**b**) maximum principal stress on the right wall of the tunnel at a depth of 100 m, (**c**) maximum principal stress on the left wall of the tunnel at a depth of 1200 m, (**d**) maximum principal stress on the right wall of the tunnel at a depth of 1200 m.

This section delves into the variations in displacement patterns, stress, and strain for deep-buried and shallow-buried tunnels under the influence of fault displacement. As the fault displacement increases, shallow-buried tunnels experience a rapid surge in stress near the fault zone, while the stress variations in deep-buried tunnels stabilize. However, the damage extent of the tunnels gradually expands. Consequently, it can be inferred that the depth effect significantly impacts the range of tunnel damage during fault displacement. Greater burial depths result in a broader damage extent.

4. Analysis of Mechanical Response Characteristics of Cross-Fault Tunnels at Different Burial Depths

To investigate the mechanical response characteristics of tunnels crossing active faults at varying burial depths, we conducted a comparative analysis of displacement patterns, stress, and strain responses for tunnel depths ranging from 100 m to 1200 m. It allowed us to summarize the damage patterns of tunnels under the influence of fault displacement at different burial depths.

As depicted in Figure 11, displacement data at the tunnel lining's crown were collected for all eight scenarios, and longitudinal distribution curves were plotted using this data. When examining the tunnel lining displacement under different conditions, it is evident that the deformations of tunnels at different burial depths still exhibit an "S"-shaped pattern. However, as the burial depth increases, the influence of the overlying stress field imposes more significant constraints on the rock mass's deformation concerning the lining. When the burial depth is 100 m or 200 m, the tunnel experiences significant bending deformation, whereas, for depths exceeding 300 m, the variation in tunnel displacement becomes less pronounced. Analysis of the displacement curves reveals that the degree of bending deformation at the tunnel deformation location gradually diminishes with increasing burial depth. Consequently, it can be inferred that as the tunnel's burial depth increases, the rock mass exerts a more significant constraint on the tunnel lining, resulting in reduced bending deformation.

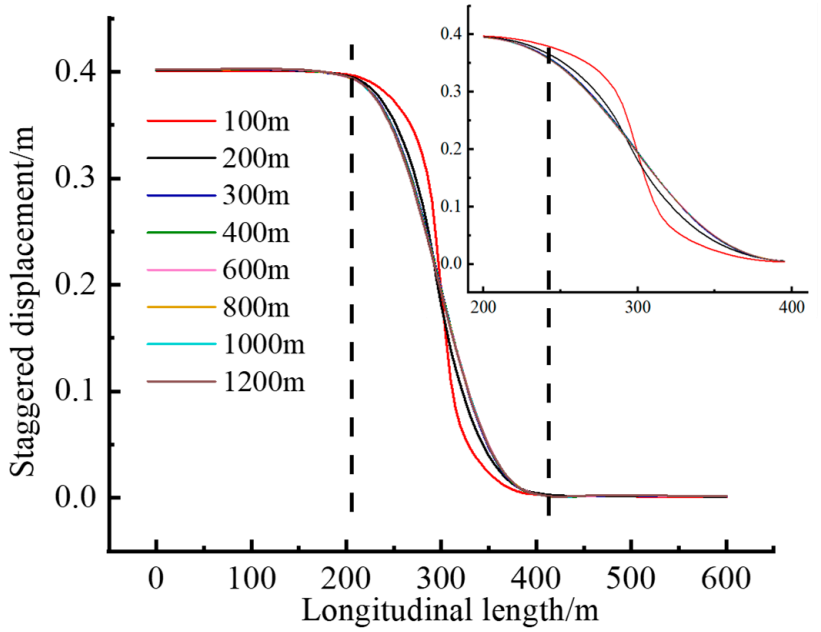

Figure 11. Displacement variation characteristics of tunnels crossing active faults at different depths.

Figure 12 shows the longitudinal distribution of the left and right wall strains in the eight cases after 0.4 m of slippage. It can be seen from the figure that the peak strains of the tunnel lining all appear in the fault zone. The peak strains of the tunnels with smaller burial depths are bigger. In contrast, the peak strains of the tunnels with larger burial depths are smaller. From the point of view of the strain characteristics of the tunnels, the

deeply buried tunnels are less affected by the misalignment effect. However, the scope of the misalignment effect is more extensive. The reason is that the environmental stress value of deeply buried tunnels is bigger, and the deformation constraint of the rock body on the tunnel lining is bigger, so the strain value of the tunnel lining is smaller when it is forced to be displaced by the rock body. In the actual project, the tunnel length should be reasonably increased for deeply buried tunnels to resist misalignment. For shallow-buried tunnels, where damage is more intensive, the number of annular reinforcement bars near the junction of the tunnel lining and the misalignment surface can be increased appropriately to resist the effects of misalignment.

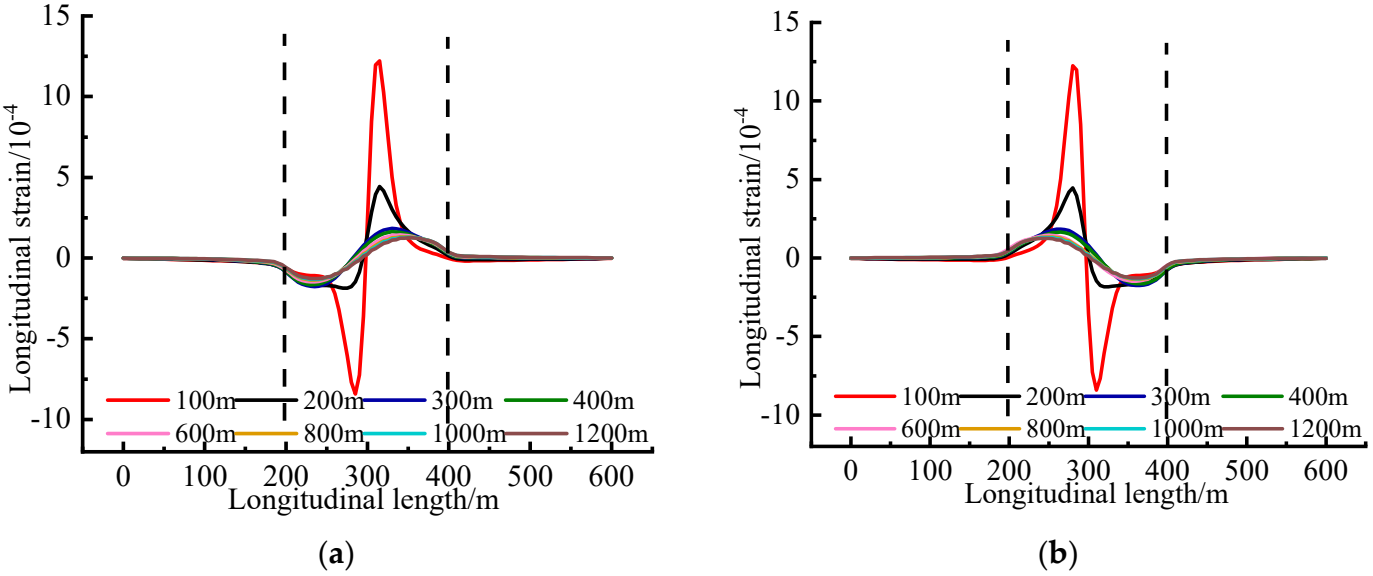

Figure 12. Strain characteristics of tunnels at different depths. (**a**) Strain on the left wall of the tunnel, (**b**) strain on the right wall of the tunnel.

Figure 13 illustrates the stress distribution on the left and right tunnel walls under the influence of fault displacement in all eight scenarios. The peak stress values are the highest for shallow-buried tunnels among all conditions. As the burial depth of the tunnel increases, the peak stress values gradually decrease. Notably, the stress variations induced by fault displacement are more significant when the tunnel is buried at depths of 100 m and 200 m. However, for depths exceeding 300 m, the stress peak values gradually decrease. In deep-burial environments, the influence of fault displacement on tunnel stress is relatively consistent, with stress peak locations nearly identical. In contrast, stress concentrations primarily occur at the fault plane in shallow-buried environments.

By examining the deformation patterns of tunnels at different burial depths, it is evident that tunnel linings exhibit an "S"-shaped deformation pattern, with the maximum deformation closely matching the fault displacement.

Notably, substantial differences in tunnel deformation are observed at 100 m and 200 m burial depths. However, as the burial depth exceeds 300 m, the influence of burial depth gradually diminishes, and the deformation pattern remains nearly constant. Similarly, tunnels' stress and strain characteristics are significantly affected by burial depth at depths of 100 m and 200 m. Nonetheless, as the burial depth surpasses 300 m, the impact of burial depth progressively decreases, resulting in a relatively stable stress and strain pattern.

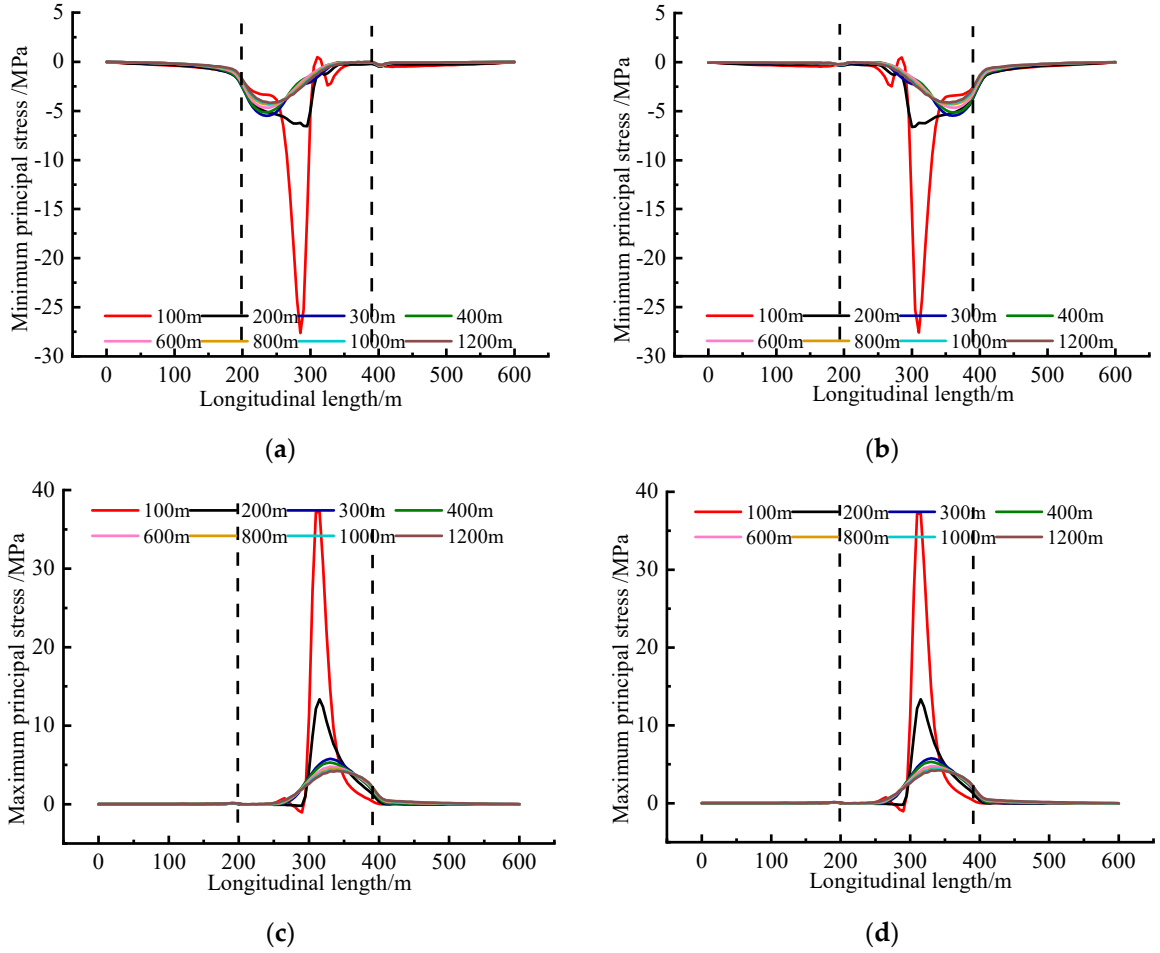

Figure 13. Stress distribution characteristics in tunnels at different depths. (**a**) Minimum principal stress on the left tunnel wall, (**b**) minimum principal stress on the right tunnel wall, (**c**) maximum principal stress on the left tunnel wall, (**d**) maximum principal stress on the right tunnel wall.

5. Conclusions

This paper presents a systematic study of deep-buried tunnels crossing active fault zones, employing numerical simulation methods to compare and analyze the differences in mechanical response characteristics between deep-buried and shallow-buried tunnels under the influence of fault displacement. Numerical simulations allow us to compare the mechanical response of deep-buried and shallow-buried tunnels under the influence of fault displacements. The study also investigates the changes in displacement patterns, stresses, and strains in tunnels at different depths, thus addressing a gap in the study of deep-buried tunnels crossing active fault zones. The main conclusions of this study are summarized below.

(1) Regarding deformation patterns, deep-buried and shallow-buried tunnels exhibit an "S"-shaped deformation characterized by bending near the fault slip surface. However, in shallow-buried tunnels, the degree of bending is more pronounced than in deep-buried tunnels. Specifically, shallow-buried tunnels experience significant deformation, albeit within a narrower distribution range, while deep-buried tunnels display a broader distribution of deformation and more extensive damage.

(2) In terms of strain distribution, the damage of the tunnel is mainly concentrated near the middle of the fault zone. After the tunnels experienced strike-slip fault movement, the shallow-buried tunnels showed similar strain patterns to the deep-buried tunnels, but their strain peaks' locations differed. However, the damage in the shallow-buried

tunnels mainly concentrates near the fault-dislocated surface, whereas the damage in the deep-buried tunnels spreads more widely throughout the fault zone.

(3) Analyzing the stress distribution within tunnels, the intense stress changes occur within the weak rock layers of the fault zone. Both shallow-buried and deep-buried tunnels experience lining failure, reaching their ultimate tensile strength when displacement reaches 0.2 m. The stress analysis confirms shear and tensile failure in the tunnel linings.

(4) When examining the damage patterns of tunnels at different burial depths, it is evident that tunnel linings are more sensitive to burial-depth effects when buried at depths of 100 m and 200 m. However, as the burial depth exceeds 300 m, the influence of burial depth on tunnel response gradually diminishes. At this point, only minimal changes occur in tunnel displacement, and there is only a slight reduction in tunnel lining stress and strain peak values with increasing burial depth.

(5) Based on the findings, practical engineering applications should involve reasonable extensions of the anti-fault protection length for deep-buried tunnels. For shallow-buried tunnels with concentrated damage, an appropriate increase in the number of circumferential steel bars near the tunnel lining and fault interface is recommended to withstand the effects of fault movement.

This study has extensively researched the mechanical response characteristics of and variations in deep-buried and shallow-buried tunnels crossing active fault zones. However, due to space limitations in this paper, specific tunnel fault mitigation measures still need to be addressed. Future research related to fault mitigation measures for deep-buried and shallow-buried tunnels will be explored.

Author Contributions: All authors contributed to the study's conception and design. J.Z. and W.Z. proposed conceptualization and methodology. J.Z. and Z.C. conducted numerical calculations and data analysis. J.Z., W.Z. and Z.C. wrote the first draft of the manuscript. All authors commented on previous versions of the manuscript. All authors have read and agreed to the published version of the manuscript.

Funding: This research received no external funding.

Data Availability Statement: The data are available by querying the authors.

Conflicts of Interest: The authors declare no conflict of interest.

References

1. Ren, R.; Zhou, H.; Hu, Z.; He, S.; Wang, X. Statistical analysis of fire accidents in Chinese highway tunnels 2000–2016. *Tunn. Undergr. Space Technol.* **2019**, *83*, 452–460. [CrossRef]
2. Zhou, W.; Qin, H.; Qiu, J.; Fan, H.; Lai, J.; Wang, K.; Wang, L. Building information modelling review with potential applications in tunnel engineering of China. *R. Soc. Open Sci.* **2017**, *4*, 170174. [CrossRef] [PubMed]
3. Roy, N.; Sarkar, R. A review of seismic damage of mountain tunnels and probable failure mechanisms. *Geotech. Geol. Eng.* **2017**, *35*, 1–28. [CrossRef]
4. Zhen, C.; Qian, S.; Zhang, G.; Zhang, M.; Mei, X. Response and mechanism of a tunnel subjected to combined fault rupture deformation and subsequent seismic excitation. *Transp. Geotech.* **2022**, *34*, 100749. [CrossRef]
5. Allen, C.R.; Luo, Z.; Qian, H.; Wen, X.; Zhou, H.; Huang, W. Field study of a highly active fault zone: The Xianshuihe fault of southwestern China. *Geol. Soc. Am. Bull.* **1991**, *103*, 1178–1199. [CrossRef]
6. McGarr, A.; Fletcher, J.B. Maximum slip in earthquake fault zones, apparent stress, and stick-slip friction. *Bull. Seismol. Soc. Am.* **2003**, *93*, 2355–2362. [CrossRef]
7. Sibson, R.H. Fault rocks and fault mechanisms. *J. Geol. Soc.* **1977**, *133*, 191–213. [CrossRef]
8. Hashash, Y.M.A.; Hook, J.J.; Schmidt, B.; Yao, J.I.C. Seismic design and analysis of underground structures. *Tunn. Undergr. Space Technol.* **2001**, *16*, 247–293. [CrossRef]
9. Shen, Y.; Gao, B.; Yang, X.; Tao, S. Seismic damage mechanism and dynamic deformation characteristic analysis of mountain tunnel after Wenchuan earthquake. *Eng. Geol.* **2014**, *180*, 85–98. [CrossRef]
10. Tsinidis, G.; de Silva, F.; Anastasopoulos, I.; Bilotta, E.; Bobet, A.; Hashash, Y.M.; He, C.; Kampas, G.; Knappett, J.; Madabhushi, G.; et al. Seismic behaviour of tunnels: From experiments to analysis. *Tunn. Undergr. Space Technol.* **2020**, *99*, 103334. [CrossRef]
11. Kenner, S.J.; Segall, P. Postseismic deformation following the 1906 San Francisco earthquake. *J. Geophys. Res. Solid Earth* **2000**, *105*, 13195–13209. [CrossRef]

12. Wang, W.L.; Wang, T.T.; Su, J.J.; Lin, C.H.; Seng, C.R.; Huang, T.H. Assessment of damage in mountain tunnels due to the Taiwan Chi-Chi Earthquake. *Tunn. Undergr. Space Technol.* **2001**, *16*, 133–150. [CrossRef]
13. Cui, G.Y.; Wang, M.N.; Yu, L.; Lin, G. Study on the characteristics and mechanism of seismic damage for tunnel structures on fault rupture zone in Wenchuan seismic disastrous area. *China Civ. Eng. J.* **2013**, *46*, 122–127.
14. Cui, G.Y.; Wu, X.G.; Wang, M.N.; Lin, G.J. Earthquake damages and characteristics of highway tunnels in the 8.0-magnitude Wenchuan earthquake. *Mod. Tunn. Technol.* **2017**, *54*, 9–16.
15. Zhang, X.; Jiang, Y.; Sugimoto, S. Seismic damage assessment of mountain tunnel: A case study on the Tawarayama tunnel due to the 2016 Kumamoto Earthquake. *Tunn. Undergr. Space Technol.* **2018**, *71*, 138–148. [CrossRef]
16. Newmark, N.M.; Hall, W.J. Pipeline design to resist large fault displacement. In Proceedings of the US National Conference on Earthquake Engineering, University of Michigan, Ann Arbor, MI, USA, 18–20 June 1975; pp. 416–425.
17. Kennedy, R.P.; Chow, A.W.; Williamson, R.A. Fault movement effects on buried oil pipeline. *Transp. Eng. J. ASCE* **1977**, *103*, 617–633. [CrossRef]
18. Yu, H.; Zhang, Z.; Chen, J.; Bobet, A.; Zhao, M.; Yuan, Y. Analytical solution for longitudinal seismic response of tunnel liners with sharp stiffness transition. *Tunn. Undergr. Space Technol.* **2018**, *77*, 103–114. [CrossRef]
19. Marco, Z.; Giuseppe, C.P.; Giuseppe, T.; Marco, S. On the influence of shallow underground structures in the evaluation of the seismic signals. *Ing. Sismica* **2021**, *38*, 23–35.
20. Zucca, M.; Valente, M. On the limitations of decoupled approach for the seismic behaviour evaluation of shallow multi-propped underground structures embedded in granular soils. *Eng. Struct.* **2020**, *211*, 110497. [CrossRef]
21. Azizkandi, A.S.; Ghavami, S.; Baziar, M.H.; Hasanaklou, S.H. Assessment of damages in fault rupture–shallow foundation interaction due to the existence of underground structures. *Tunn. Undergr. Space Technol.* **2019**, *89*, 222–237. [CrossRef]
22. Banushi, G.; Squeglia, N.; Thiele, K. Innovative analysis of a buried operating pipeline subjected to strike-slip fault movement. *Soil Dyn. Earthq. Eng.* **2018**, *107*, 234–249. [CrossRef]
23. Wang, Z.Z.; Zhang, Z.; Gao, B. The seismic behavior of the tunnel across active fault. In Proceedings of the 15th World Conference on Earthquake Engineering, Lisbon, Portugal, 24–28 September 2012; pp. 1–7.
24. Sabagh, M.; Ghalandarzadeh, A. Centrifugal modeling of continuous shallow tunnels at active normal faults intersection. *Transp. Geotech.* **2020**, *22*, 100325. [CrossRef]
25. Huang, F.; Wu, C.; Ni, P.; Wan, G.; Zheng, A.; Jang, B.A.; Karekal, S. Experimental analysis of progressive failure behavior of rock tunnel with a fault zone using non-contact dic technique. *Int. J. Rock Mech. Min. Sci.* **2020**, *132*, 104355. [CrossRef]
26. Zhou, G.; Sheng, Q.; Cui, Z.; Wang, T.; Ma, Y. Investigating the deformation and failure mechanism of a submarine tunnel with flexible joints subjected to strike-slip Faults. *J. Mar. Sci. Eng.* **2021**, *9*, 1412. [CrossRef]
27. Wang, T.; Geng, P.; Li, P.; Wang, Q.; Wang, L. Deformation and failure of overburden soil subjected to normal fault dislocation and its impact on tunnel. *Eng. Fail. Anal.* **2022**, *142*, 106747. [CrossRef]
28. Zhang, Y.; Zhang, Z.; Yin, C.; Wei, R.; Zhang, H. Experimental study on forced response characteristics and anti-dislocation performance of articulated tunnel structure under dislocation action of normal fault. *Structures* **2023**, *48*, 867–881. [CrossRef]
29. Zhao, W.; Gao, H.; Chen, W.; Liu, J.; Peng, W.; Zhou, S. Effects of the friction coefficient and location of the dislocation surface of an active fault on the mechanical response of a freeway tunnel. *Environ. Earth Sci.* **2023**, *82*, 288. [CrossRef]
30. Zhou, H.; Zhao, H.T.; Li, J.; Zhao, C.W.; Liu, W.B.; Zhang, C.Q.; Wang, Y.Z. Creep Characteristics and Dislocation Mode of the West Branch of Longpan-Qiaohou Fault in Xianglushan Tunnel. *J. Yangtze River Sci. Res. Inst.* **2022**, *39*, 97–104. (In Chinese)
31. *GB 50010-2010*; Code for Design of Concrete Structures. China Architecture & Building Press: Beijing, China, 2010. (In Chinese)

Disclaimer/Publisher's Note: The statements, opinions and data contained in all publications are solely those of the individual author(s) and contributor(s) and not of MDPI and/or the editor(s). MDPI and/or the editor(s) disclaim responsibility for any injury to people or property resulting from any ideas, methods, instructions or products referred to in the content.